Nuclear Instruments and Methods in Physics Research B 486 (2021) 1–10

Contents lists available at ScienceDirect

Nuclear Inst. and Methods in Physics Research, B

journal homepage: www.elsevier.com/locate/nimb

TEM analysis of radiation effects in ODS steels induced by swift heavy ions

Sergey V. Rogozhkin [a,b,*], Aleksei A. Bogachev [a,b], Alexander A. Nikitin [a,b], Alexander L. Vasiliev [c], Michael Yu. Presnyakov [c], Marilena Tomut [d,e], Christina Trautmann [d,f]

[a] Institute for Theoretical and Experimental Physics Named By A.I. Alikhanov of National Research Centre «Kurchatov Institute», 117218 Moscow, Russia
[b] National Research Nuclear University MEPhI, 115409 Moscow, Russia
[c] National Research Center "Kurchatov Institute", 123182 Moscow, Russia
[d] GSI Helmholtzzentrum für Schwerionenforschung, 64291 Darmstadt, Germany
[e] Institute of Materials Physics, WWU Münster, 48149 Münster, Germany
[f] Technische Universität Darmstadt, 64277 Darmstadt, Germany

ARTICLE INFO

Keywords:
Swift heavy ion irradiation
ODS steels
Oxide inclusion
Track

ABSTRACT

Oxide dispersion strengthened steels ODS Eurofer and ODS 13.5Cr-0.3Ti were irradiated with 945 MeV Au ions and 167 MeV Xe ions at room temperature. Beam-induced microstructural changes were analyzed by high-resolution transmission electron microscopy in the region of maximum electronic energy loss of 55 and 30 keV/nm, respectively.

In both ODS steels, an increase in the fraction of small oxide inclusions (<5 nm) was observed. In ODS Eurofer steel, the irradiation with Xe and Au ions leads to the formation of amorphous tracks in yttrium oxide inclusions larger than 8 nm with track diameters of 2 nm and 3–4 nm, respectively.

1. Introduction

Ferritic-martensitic steels reinforced by inclusions of secondary phases such as carbonitrides or oxides are most promising materials for the core of advanced nuclear power plants. Oxide dispersion strengthened (ODS) alloys are being developed to be used in extreme temperature and nuclear environments. In space, e.g., these materials can be subjected to both low and high-energy particles from cosmic radiation, and in nuclear power plants the material is exposed to neutron radiation and energetic fission fragments. The high-temperature strength and irradiation resistance originate from the ability of ODS inclusions to pin dislocations and in turn prevent creep. The properties of ODS steels are highly dependent on the characteristics of the oxide inclusions.

In this study, ODS steels were irradiated with swift heavy ions to analyze the radiation hardness of oxide inclusions. When swift heavy ions (kinetic energy in the MeV to GeV range) slow down in a solid, they cause intense electronic excitation, ionization processes and damages along their trajectory.

In many materials, in particular in insulators, the high energy deposition by the ion projectile leads to the creation of so-call tracks. Tracks consists of structurally modified or completely amorphized material. Track formation requires a critical electronic energy loss (dE/dx) which depends on the material and is low for organic insulators and high for most metals [1–3]. If the deposited energy is insufficient for track formation, point defects or defect clusters may appear in the close vicinity of the ion trajectory. In supersaturated solid solutions, the nucleation of clusters and nanoscale precipitates was reported (see for example, [4]). Resistance to track formation is high for metals due to the high mobility of the electrons, resulting in energy transport away from the ion trajectory before the energy can be transferred to the atoms [5]. In a variety of metals (Cu, Au, Ag, etc.) tracks are obviously not formed. In pure Fe irradiated with 18–40 MeV C_{60} cluster ions of highest electronic energy losses (52–91 keV/nm, respectively), some defect structures were observed that were attributed to dislocation lines oriented along the ion path [6].

In recent years, radiation effects induced by swift heavy ions have been studied in a large variety of materials including metals, semiconductors, and dielectrics. Also track formation models have been proposed and are continuously refined [7–9].

Regarding nanostructured heterogeneous materials, it is important to improve the understanding of radiation effects related to the size of inclusions that can be comparable to the size of ion tracks. In this case, defect creation as well as of track formation processes can be modified due to the change in efficiency of the transfer of the deposited energy

* Corresponding author at: Bolshaya Cheremushkinskaya st., 25, 117218 Moscow, Russia.
E-mail address: Sergey.Rogozhkin@itep.ru (S.V. Rogozhkin).

https://doi.org/10.1016/j.nimb.2020.10.017
Received 26 June 2020; Received in revised form 21 September 2020; Accepted 27 October 2020
0168-583X/

Table 1
Nominal chemical composition of the ODS steels of our study (at.%).

Material	Cr	Ti	Y	O	V	Mn	Si	C	N
ODS Eurofer [16,17]	9.65	–	0.25	0.37	0.38	0.38	0.16	0.51	0.03
ODS 13.5Cr–0.3Ti [18]	14.60	0.35	0.15	0.22	–	–	–	–	–

from irradiated inclusions into the surrounding matrix.

Amorphization of the metallic matrix was not detected in any ODS steels exposed to swift heavy ion irradiation. However, instabilities of reinforcing inclusions in these steels have recently been found. The formation of amorphous tracks was reported to depend on the size and nature of the oxide inclusions [10]. In KP4 (Fe–15Cr–4Al–2W–0.35Y_2O_3) ODS alloy (Kyoto University, Japan), small inclusions up to 5 nm remained stable after irradiation with 700 MeV Bi ions up to a fluence of 1.5×10^{13} cm^{-2}, whereas after irradiation with 167 MeV Xe ions of fluence 1.5×10^{15} cm^{-2} those small inclusions were partially amorphized. Irradiation of Fe-16Cr-3 W ODS steel (VNIINM, Moscow) with 700 MeV Bi ions of 1.5×10^{13} cm^{-2} led to the formation of overlapping tracks in $(Cr, W)_{23}C_6$, $Y_2Ti_2O_7$ and Y_2TiO_5 inclusions and their complete amorphization.

The formation of amorphous tracks in Y-Ti-O and $Cr_{23}C_6$ inclusions was studied in detail in [10–12]. Samples of EP-450 (Fe–13Cr–2Mo–Nb–V–B–0.12C) ODS steel (VNIINM, Moscow) were irradiated with 167 MeV and 220 MeV Xe ions, 700 MeV Bi, 48 MeV Ar, and 107 MeV Kr ions at temperatures between 30 and 650 °C corresponding to energy losses between 3.6 and 24.3 keV/nm. Both Kr and Xe ion irradiations led to the formation of amorphous tracks in $Y_2Ti_2O_7$ oxides in EP450 ODS steel. Analysis by high-resolution transmission electron microscopy (TEM) showed that the track size in the $Y_2Ti_2O_7$ inclusions increases linearly with energy losses and the threshold for track formation is between 7.4 and 9.7 keV/nm.

Amorphization of oxide inclusions can occur both as a result of excitation of the electronic subsystem and due to elastic collision cascades. In the study of Lescoat et al. [13], EM10 ODS (Fe–9Cr–1Mo) and DY ODS (Fe–13Cr–1.5Mo) reinforced respectively by mixed yttrium-titanium oxides and magnesium oxides were irradiated with 92 MeV Xe ions at room temperature (RT) to 3.2×10^{14} cm^{-2} and also with 700 keV Kr^{2+} and 1.2 MeV Kr^{3+} ions up to 100 dpa in the temperature range of 300–600 °C. TEM analysis of the steels irradiated with 92 MeV Xe ions showed both amorphized and crystalline inclusions. The irradiation of DY ODS steel with 1.2 MeV Kr ions to 45 dpa at a temperature of<500 °C led to amorphization of Y-Ti-O inclusions, while Y-O and Ti-O inclusions in the same material revealed no damage. It was shown that amorphization due to elastic collisions depends on the nature of the inclusion as well as on dose and irradiation temperature. A TEM study of DY ODS and Fe-18Cr-1 W-0.3Ti-0.5Y_2O_3 steels irradiated with 74 MeV Kr ions up to 10^{12} cm^{-2} at RT revealed amorphization of oxide Y-Ti-O inclusions due to multiple overlap of tracks [14].

A number of studies showed that the temperature during irradiation has a direct effect on the amorphization of oxides in ODS materials. In case of irradiation of DY ODS with 1.2 MeV Kr^{3+} ions up to 44 dpa at or above 500 °C, amorphization was completely suppressed and the number of oxides with a damaged interface layer between the matrix and inclusion increased [13]. Temperature also affects the amorphization of oxide inclusions under high-energy irradiation [15,16]. Amorphization of $Y_2Ti_2O_7$ inclusions in Fe-18Cr-1 W-0.3Ti-0.5Y_2O_3 steel observed after irradiation with 92 MeV Xe ions to 3×10^{14} cm^{-2} at RT was suppressed when increasing the irradiation temperature to 500 °C [17].

To date, studies on ODS materials under swift heavy ions are scarce and not systematic. Novel ODS alloys contain only small oxide inclusions (<10 nm) and the influence of swift heavy ion irradiation on these inclusions has not yet been investigated in details. The aim of this study is to identify details of beam-induced modifications of oxide inclusions of different sizes in ODS steels under swift heavy ion irradiation of various energy loss and ion fluences.

Table 2
Characteristics of microstructural features of as-received ODS Eurofer and ODS 13.5Cr-0.3Ti steels obtained by transmission electron microscopy (FEI Tecnai F20 microscope).

	ODS Eurofer	ODS 13,5Cr-0,3Ti
Ferrite grain size, μm	4–7	6–8
Martensite graine size, μm	–	0.1–0.7
Oxide size*, nm	11 ± 6	5 ± 2
Number density of oxides, m^{-3}	$(5 \pm 1) \times 10^{21}$	$(3.0 \pm 0.3) \times 10^{22}$

* The diameter of circle that fully overlapped the particle was chosen as the oxide size.

2. Materials

In the present work, ODS Eurofer [18,19] and ODS 13.5Cr–0.3Ti steel [20] are studied. The first-generation ODS Eurofer steel by Planzee, an Austrian industrial group, was produced by mechanical alloying of Eurofer 97 master steel with 0.5 wt% yttrium oxide powder. ODS 13.5Cr–0.3Ti steel was developed and manufactured by powder metallurgy at the Karlsruhe Institute of Technology (Germany). The mechanical alloying was carried out in an attritor mill in argon atmosphere for ODS Eurofer steel and in hydrogen atmosphere for ODS 13.5Cr–0.3Ti steel. The ODS Eurofer steel was subjected to hot isostatic pressing (HIP) at a pressure of 100 MPa and a temperature of 1150 °C. The compaction of ODS 13.5Cr–0.3Ti steel was carried out by hot extrusion at 1100 °C. ODS Eurofer steel was additionally subjected to high-temperature treatment with annealing for 30 min at 980 °C and tempering for 2 h at 760 °C. The nominal chemical composition of the studied materials is presented in Table 1. The density of ODS Eurofer and ODS 13.5Cr–0.3Ti steels are 7.805 g/cm^3 and 7.768 g/cm^3, respectively.

The results of a quantitative analysis by transmission electron microscopy of the microstructural features for ODS Eurofer and ODS 13.5Cr-0.3Ti steels are presented in Table 2. The materials contain a large number of nanoscale oxide inclusions which are identically oriented whithin a given grain. In ODS Eurofer steel, oxide inclusions larger than 10 nm have a stoichiometry of Y_2O_3 [21,22], and in ODS 13.5Cr-0.3Ti steel the stoichiometry of large Y-Ti-O inclusions is $Y_2Ti_2O_7$ [20]. The typical sizes of the oxide inclusions (3 – 7 nm) in ODS 13.5Cr-0.3Ti steel are two times smaller than the oxides in ODS Eurofer (5 – 17 nm). Besides the large number of oxide inclusions smaller than 20 nm, ODS Eurofer steel also contains a few large oxides with a size up to 80 nm. The size distributions of oxide inclusions in as-received steels as shown in Fig. 1 differ markedly. The different oxide sizes allows us to test differences in radiation stability and heat transfer efficiency of these nanosized inclusions.

3. Irradiation experiments

The samples had the form of disks with a diameter of 3 mm and a thickness of ~120 μm obtained by electrical discharge machining and subsequent mechanical thinning. The surface roughness of the samples was measured by atomic force microscopy and did not exceed 10 nm.

The irradiations were performed at RT with 167 MeV Xe ions of fluence 1×10^{13} cm^{-2} and 1×10^{14} cm^{-2} at the accelerators IC-100 (JINR, Dubna) and with 945 MeV Au ions of fluence 1×10^{11} cm^{-2}, 5×10^{12} cm^{-2}, and 1×10^{13} cm^{-2} at the UNILAC (GSI, Darmstadt).

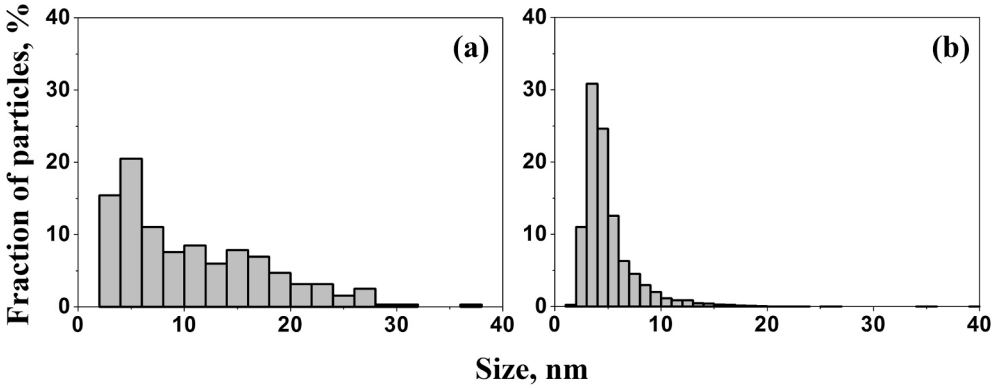

Fig. 1. Size distributions of oxide inclusions in as-received steels: (a) ODS Eurofer; (b) ODS 13.5Cr-0.3Ti from TEM analysis.

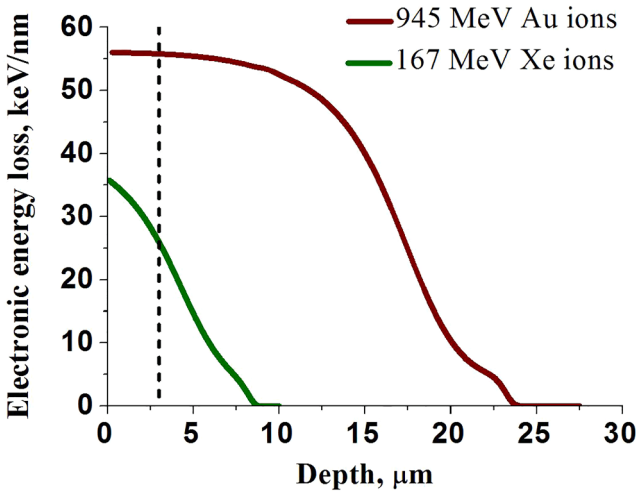

Fig. 2. Electronic energy loss as a function of penetration depth for 945 MeV Au ions (upper brown line) and 167 MeV Xe ions (low green line) in pure iron. The calculation was performed with the SRIM-2008 code [23]. The vertical dashed lines indicate the depth at which the samples were analysed by TEM corresponding to an energy reduced to 115 MeV (Xe) and 855 MeV (Au). (Colored image for online version).

The electronic energy loss of 167 MeV Xe and 945 MeV Au ions as a function of depth in Fe (7.865 g/cm^3) is shown in Fig. 2. For the calculation of the range and energy loss, the SRIM-2008 code was used [23]. To avoid the defects induced by mechanical preparation of the sample and the influence of the surface as a sink of irradiation defects, the TEM analysis was carried out at a depth of ~3 μm indicated by the vertical dash lines on Fig. 2. At this depth, the electronic energy loss in pure Fe is ~30 keV/nm for Xe ions and ~56 keV/nm for Au ions. According to SRIM calculations, the energy of the Xe and Au ions at a depth of 3 μm from the irradiated surface of the steel sample is 115 MeV and 855 MeV, respectively and the corresponding to electronic energy loss in Y_2O_3 (4.860 g/cm^3) is ~16 keV/nm for Xe ions and 30 keV/nm for Au ions. These values are far above the threshold for track formation of 7.4–9.7 keV/nm reported for yttrium oxide inclusions in a similar steel EP-450 ODS [24].

4. TEM sample preparation and methods

TEM specimens were prepared by electrochemical thinning irradiated samples on a TenuPol-5 device using a 20% solution of sulfuric acid in methanol as electrolyte. The temperature of the electrolyte was 18 °C and a voltage of 12 V was applied to the sample. By precision thinning, a 3 ± 1 μm thick material layer was removed from the irradiated sample

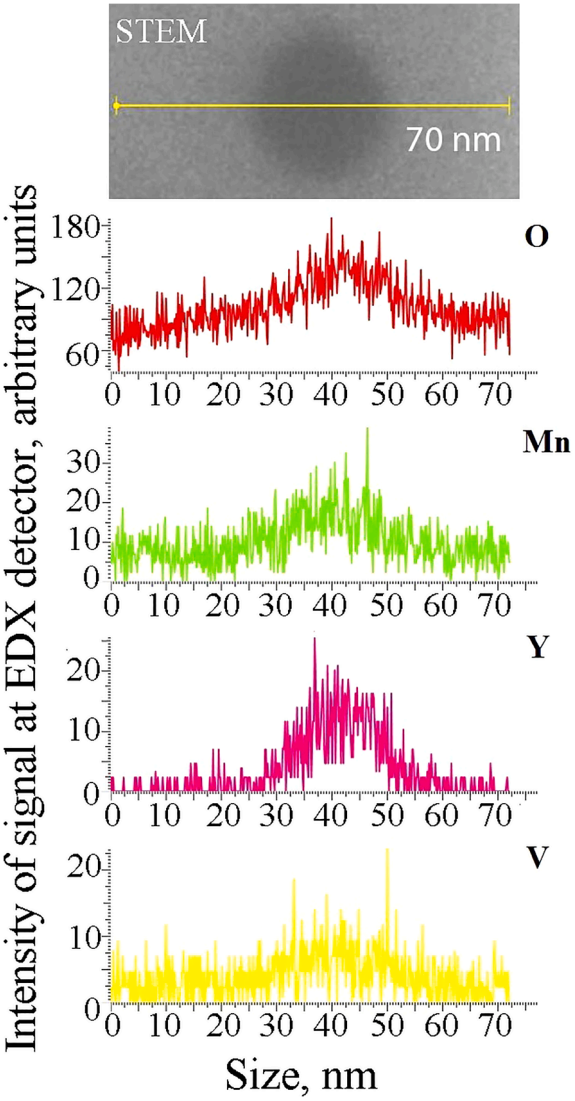

Fig. 3. Scanning TEM image of a single $(Y_{1.8}Mn_{0.2})O_3$ oxide inclusion of a ODS Eurofer sample irradiated with Au ions to 5 × 10^{12} cm^{-2} (top) and corresponding chemical composition signals recorded by line scan analysis using energy dispersive X-ray (EDX) spectroscopy (bottom). (Colored image for online version).

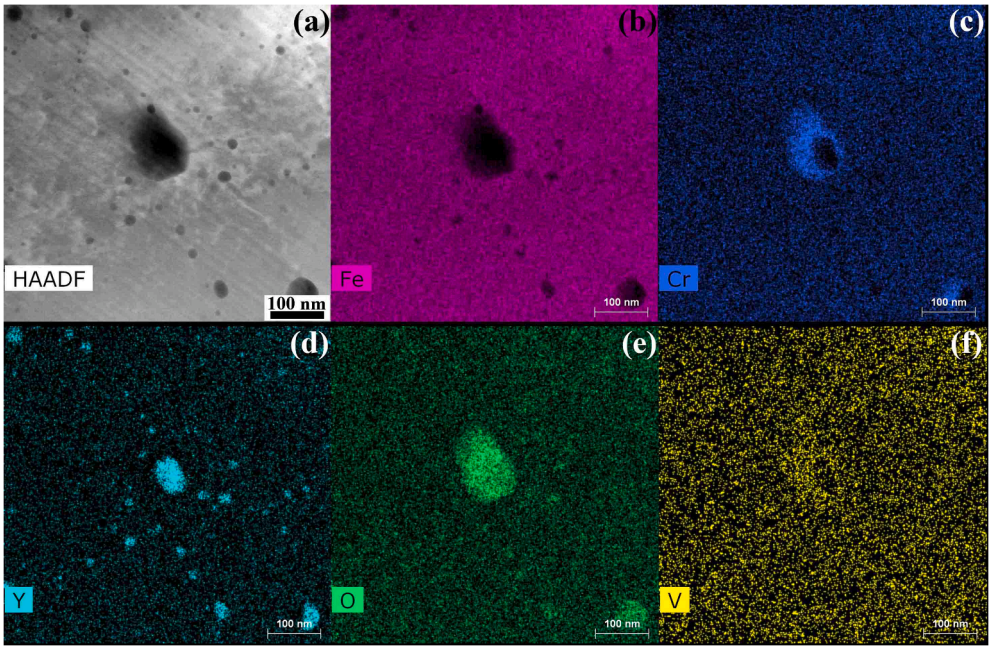

Fig. 4. EDX elemental mapping of area in ODS Eurofer irradiated with Au ions to 10^{13} cm^{-2}: (a) HAADF image, (b)–(f) elemental maps obtained using Fe-K, Cr-K, Y–L, O–K, and V-K EDX lines, respectively. (Colored image for online version).

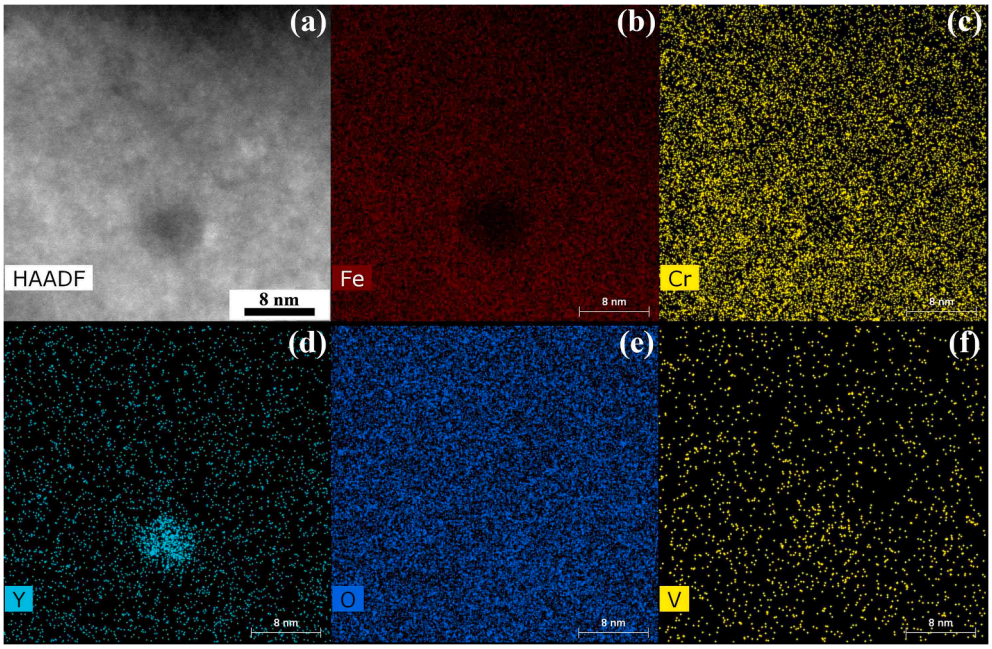

Fig. 5. EDX elemental mapping of nano-oxide in ODS Eurofer irradiated with Au ions to 10^{13} cm^{-2}: (a) HAADF image, (b)–(f) elemental maps obtained using Fe-K, Cr-K, Y–L, O–K, and V-K EDX lines, respectively. (Colored image for online version).

surface. The etching depth of the material was controlled using a PROFI-130 profilometer. Final thinning was carried out on the un-irradiated side of the sample until the electron beam of the TEM was able to transmit the thinned material layer. In this last process step, the ion-irradiated surface was isolated from the electrolyte using a protective film.

In addition, TEM samples were prepared with a focused Ga^+ ion beam at a Helios NanoLab 600 (FEI) scanning microscope at an accelerating voltage of 5–30 kV. Cross sections from the ion-irradiated samples along the beam direction as well as a longitudinal section on a depth of ~3 μm below the initial surface were obtained.

TEM samples prepared by electrochemical thinning were analysed using a JEOL JEM-2100 and a FEI Tecnai F20 transmission electron microscope operated at an accelerating voltage of 200 keV. The lamellae cut by focused ion beam were studied using a Titan 80–300 (FEI) and Tecnai Osiris S/TEM (FEI) microscopes at an accelerating voltage of 300 keV and 200 keV respectively. Qualitative chemical analysis of the TEM samples was carried out by X-ray energy dispersive spectroscopy using a Si (Li) detector (EDAX) and SuperX spectrometer with 4 silicon drift detectors.

For the analysis of the number density of the inclusions, the local thickness of TEM samples was determined by EELS measurements using

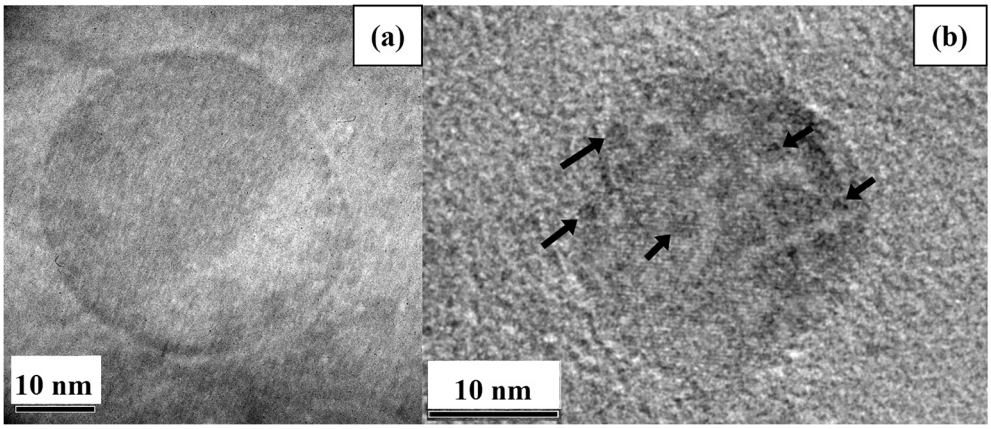

Fig. 6. Bright-field TEM images of ODS Eurofer steel samples: (a) unirradiated and (b) irradiated with Xe ions to a fluence of 10^{13} cm^{-2}. The arrows indicate tracks within the large Y_2O_3 inclusion.

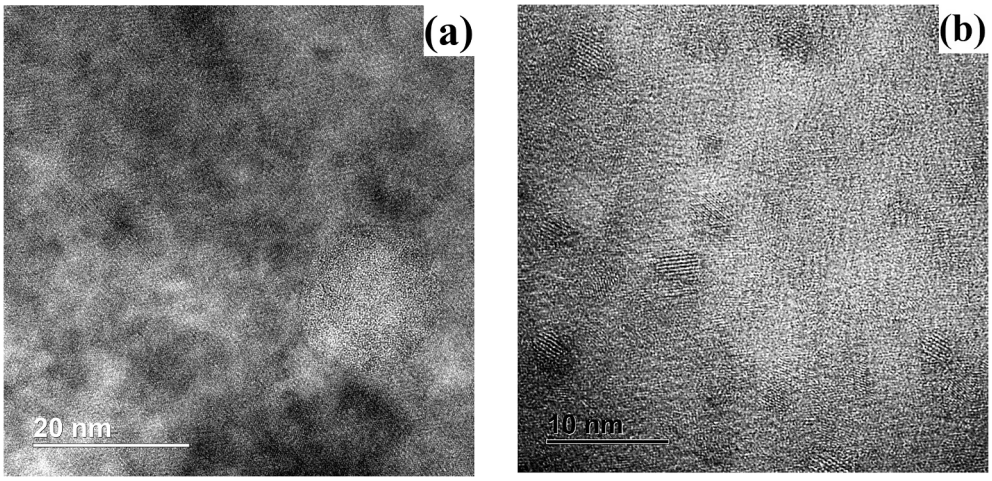

Fig. 7. HRTEM images of oxide inclusions in the steels: (a) ODS Eurofer irradiated with Au ions to 10^{13} cm^{-2} and (b) ODS 13.5Cr – 0.3Ti irradiated with Au ions to 5×10^{12} cm^{-2}.

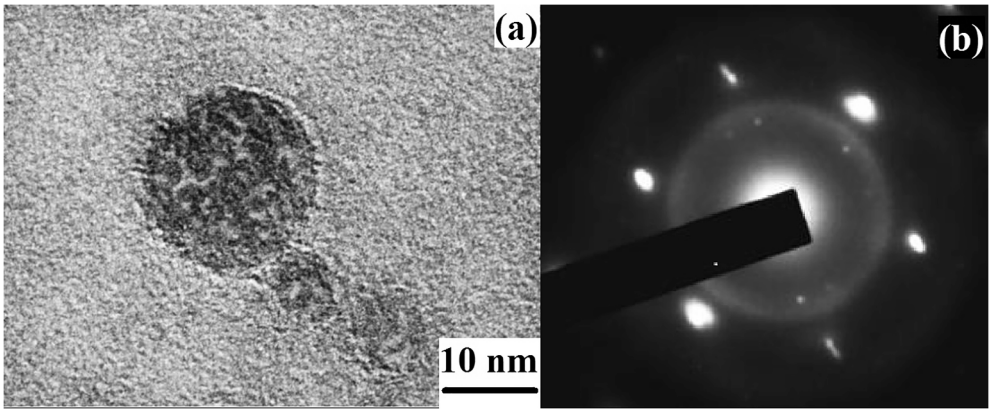

Fig. 8. ODS Eurofer irradiated with Xe ions to 10^{13} cm^{-2}: (a) Representative high-resolution TEM image of large Y_2O_3 inclusion containing ion tracks. (b) Diffraction pattern from the oxide inclusion where the diffuse halo ring indicates amorphization. Images were obtained with a JEOL JEM-2100 microscope at an accelerating voltage of 200 keV.

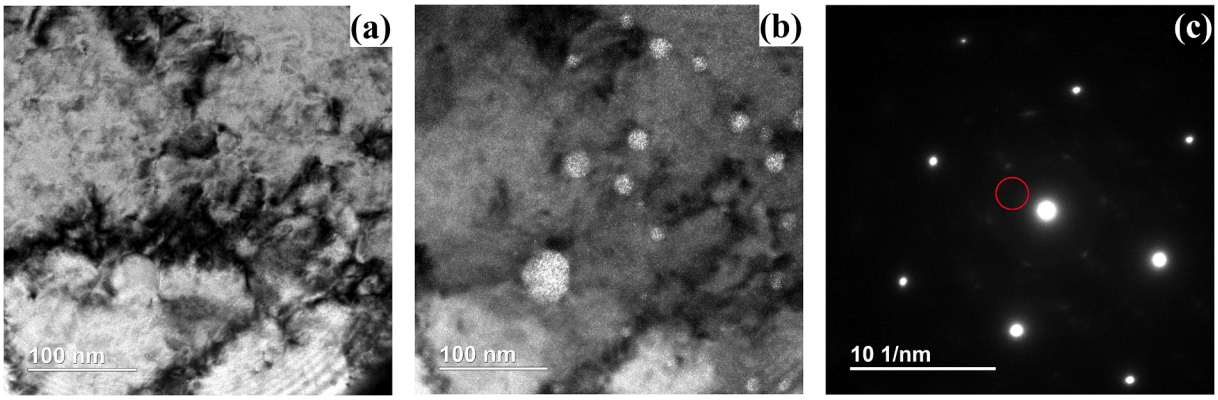

Fig. 9. ODS Eurofer irradiated with Au ions to 10^{13} cm^{-2}: (a) representative bright-field TEM image; (b) dark-field TEM image from selected area on diffraction pattern; (c) diffraction pattern from amorphous oxide inclusions with selected area (circle). Images were obtained with Tecnai Osiris S/TEM (FEI) microscope at an accelerating voltage of 200 keV. (Colored image for online version).

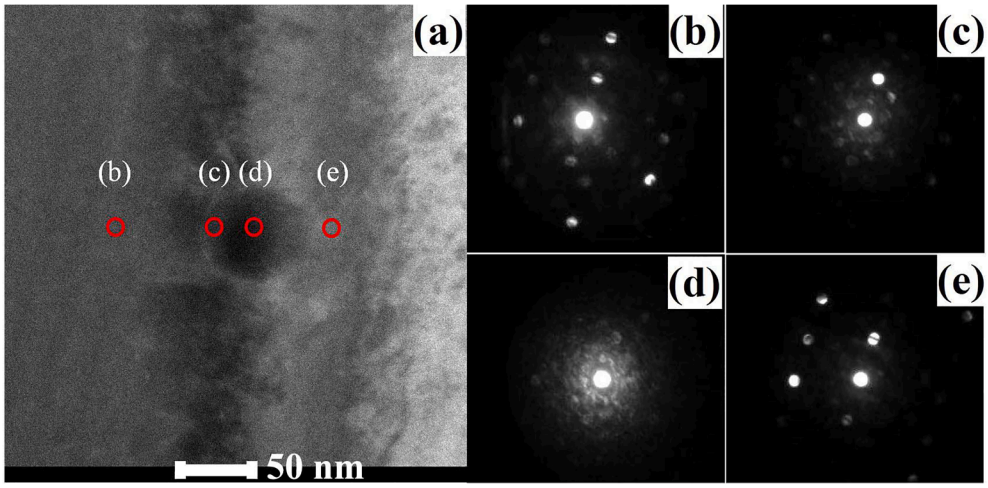

Fig. 10. ODS Eurofer sample irradiated with Au ions to 5×10^{12} cm^{-2}: (a) representative bright-field TEM image of sample cross-section (cut normal to the irradiated surface) showing a severely damaged oxide inclusion; (b)-(e) diffraction patterns in selected areas as indicated in (a). The diffuse halo ring in Figure (d) indicates amorphization while the surrounding matrix (b, e) is crystalline. The interface between oxide and matrix (c) is partly amorphized. Images were obtained using a Titan 80–300 (FEI) microscope at an accelerating voltage of 300 keV. (Colored image for online version).

the zero loss peak. For each sample, at least 6 thickness measurements at different positions were performed. The average thickness for all investigated samples was about (100 ± 10) nm.

5. Results

Energy dispersive X-ray (EDX) spectroscopy in combination with scanning TEM imaging confirms that the studied inclusions are yttrium oxides with a low content of manganese and vanadium (Fig. 3). As reported in [22], the cores of the yttrium oxides in ODS Eurofer consist of a $(Y_{1.8}Mn_{0.2})O_3$ phase which is surrounded by a 0.5–1.5 nm vanadium and chromium enriched shell. EDX-mapping showed that all detected nanoparticles, regardless size, consist of Y and O (Fig. 4). Large oxides also have Cr and V enriched shell. The O contrast was insufficient for small oxides (see Fig. 5). Noticeable changes in the chemical composition of oxides after the ion irradiation were not detected.

Ion-beam induced rearrangements of oxide inclusions in irradiated ODS Eurofer samples detected by high-resolution electron microscopy are presented in Figs. 6-10. To detect radiation-induced amorphization of the inclusions, electron diffraction images were recorded (see Fig. 8b, 9c, 10b-10e).

In the TEM images of all irradiated ODS Eurofer steel samples, oxide inclusions larger than about 8 nm contain amorphous regions in the form of separate or intersecting areas. This microscopic observation is supported by the appearance of an amorphous halo in the diffractograms (Fig. 8b, 10d). Darkfield image with bright amorphous oxides on Fig. 9b corresponds to area of amorphous halo on diffraction pattern (Fig. 9c). On Fig. 10 diffraction patterns along the line are represented to show the transition between lattice (Fig. 10b, 10e) and amorphous region (Fig. 10c, 10d). This set of images was obtained using nanoarea electron diffraction technique. We conclude that the separate round amorphous areas are ion tracks embedded in the crystalline Y_2O_3 inclusions. Intersecting amorphous areas is the result of tracks overlapping. Large oxides in the steel irradiated with Au ions to 10^{13} $cm^{-2}$and Xe ions to 10^{14} cm^{-2} were fully amorphous due to tracks overlapping. No signs of amorphization or track formation were identified for oxides smaller than 8 nm

Table 3
Average size and number density of Y_2O_3 inclusions and ion tracks in large oxides in ODS Eurofer steel irradiated with 855 MeV Au and 115 MeV Xe ions of different fluences. The quantitative analysis was carried out using TEM (FEI Tecnai F20) images.

Type of ions	Au			Xe	
Fluence, cm^{-2}	1×10^{11}	5×10^{12}	1×10^{13}	1×10^{13}	1×10^{14}
Oxide size, nm	3 ± 1	4 ± 2	4 ± 2	3 ± 1	5 ± 3
Oxide number density, 10^{22} m^{-3}	7.0 ± 0.7	6.0 ± 0.6	6.0 ± 0.6	1.2 ± 0.3	1.3 ± 0.2
Track diameter, nm	3 ± 1	4 ± 1*	4 ± 1*	2 ± 1*	2 ± 1*
Track density, cm^{-2}	5×10^{11}	4×10^{12}*	–	1×10^{13}*	–

* For non-overlapped or well-separated tracks.

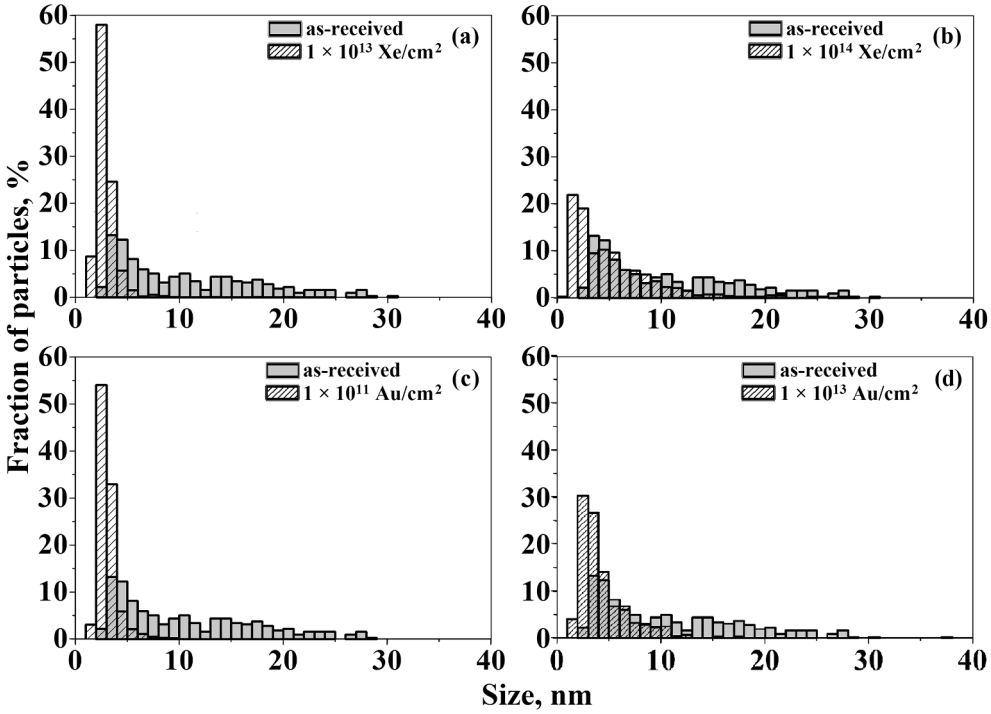

Fig. 11. Size distribution of oxide inclusions in ODS Eurofer before (gray) and after irradiation (shaded) with Xe ions to: (a) 1×10^{13} cm^{-2}; (b) 1×10^{14} cm^{-2} and with Au ions to: (c) 1×10^{11} cm^{-2}; (d) 1×10^{13} cm^{-2}.

(Fig. 7a). Also no amorphous regions or any irradiation-induced defects were found in the steel matrix.

A quantitative analysis of these regions is presented in Table 3. The track size was estimated as a diameter of circle, which fully overlapped separate round amorphous area. In spite of the fact that the tracks should be partially overlapped for Au irradiation to 5×10^{12} cm^{-2} and Xe irradiation to 1×10^{13} cm^{-2}, separated tracks were also observed in oxide inclusions. The number density and size of the tracks in the Table 3 were estimated for non-overlapped or well-separated tracks. The number density of tracks for samples irradiated with Au ions to 10^{13} cm^{-2} and with Xe ions to 10^{14} cm^{-2} can't be estimated because of severe track overlapping. The track size in these samples was qualitative estimated from several detected non-overlapped tracks.

The electronic energy loss of 115 MeV Xe (~16 keV/nm) and 855 MeV Au (30 keV/nm) ions in yttrium oxide inclusions significantly exceeds the threshold (7.4–9.7 keV/nm) for track formation reported in [23]. The track size for Au ions (3–4 nm) is larger than for Xe ions (2 nm) which is in full agreement with the common observation that the size of tracks gets larger with increasing energy loss.

The results of a quantitative analysis of oxide inclusions in ODS Eurofer steel after irradiation are included in Table 3. For analysis, the diameter of circle that fully overlaps the inclusion was accepted as the size of oxide. The respective size distributions before and after ion irradiation of more than 500 analyzed oxide inclusions are presented in Fig. 11. After the irradiation with Au ions to 10^{11} cm^{-2} and with Xe ions to 10^{13} cm^{-2}, the fraction of small inclusions (<5 nm) is larger and large oxides have dissolved. For higher fluences (10^{13} Au/cm^2 and 10^{14} Xe/cm^2), the increase of fraction of small oxides not so pronounced.

Representative examples of inclusions observed after different irradiations are shown at Fig. 12. For all investigated states of the ODS Eurofer samples, the TEM images show a uniform distribution of the oxides. No agglomerations of inclusions or empty areas within the grains are found.

TEM images of ODS 13.5Cr – 0.3Ti steel irradiated with Au and Xe ions up to 5×10^{12} cm^{-2} and 10^{14} cm^{-2} are shown in Fig. 13. High-resolution transmission microscopy did not reveal any signs of irradiation-induced amorphization or defects in the steel matrix and within the oxide particles (Fig. 7b). The spatial distribution of the inclusions within the grain remains stable after irradiation, without areas of agglomeration or lack of inclusions.

The analysis of size distribution of oxide inclusions reveals that the number of oxides with a size of <5 nm is increased under ion irradiation (Fig. 14). The larger fraction of small oxides can be caused by partial dissolution of large oxides during irradiation. Table 4 demonstrates the significant decrease in average size and an increase in the number density of oxides after irradiation.

6. Discussion

In large oxide inclusions (greater than8 nm) in ODS Eurofer steel, the formation of amorphous tracks is detected, whereas this effect does not occur in ODS 13.5Cr–0.3Ti steel, which in the pristine state contains mainly Y-Ti-O oxides smaller than 5 nm. It can be assumed that the larger surface-to-bulk ratio of smaller inclusions provides a more efficient transfer of the deposited energy to the matrix and thus suppresses track formation in the oxide inclusions.

TEM analysis of both ODS steels shows that the irradiation with 167 MeV Xe and 945 MeV Au ions results in a decrease of the average size of the oxide inclusions and to an increase of the fraction of small oxides (<5 nm). After irradiation also the total number density of oxides increased in all investigated states of ODS Eurofer (Fig. 15a) and ODS 13.5Cr – 0.3Ti (Fig. 15b). This effect is ascribed to the large electronic energy loss of the Xe ions (~16 keV/nm) and Au ions (30 keV/nm) in yttrium oxides leading to a partial dissolution of initially larger particles. After irradiation the overall distribution of the oxides in the steels remains uniform and there is no obvious agglomeration (such as halo effect) of oxide particles observed.

It should be noted that an increased number density of small (<5 nm) oxide inclusions was observed in ODS steels under low-energy heavy ion irradiation (5.6 MeV Fe^{2+} and 4.8 MeV Ti^{2+}) where the energy loss due to elastic collisions prevails [25]. We ascribe the reason for the increase of oxide particles during heavy ion irradiation to nanoscale cluster

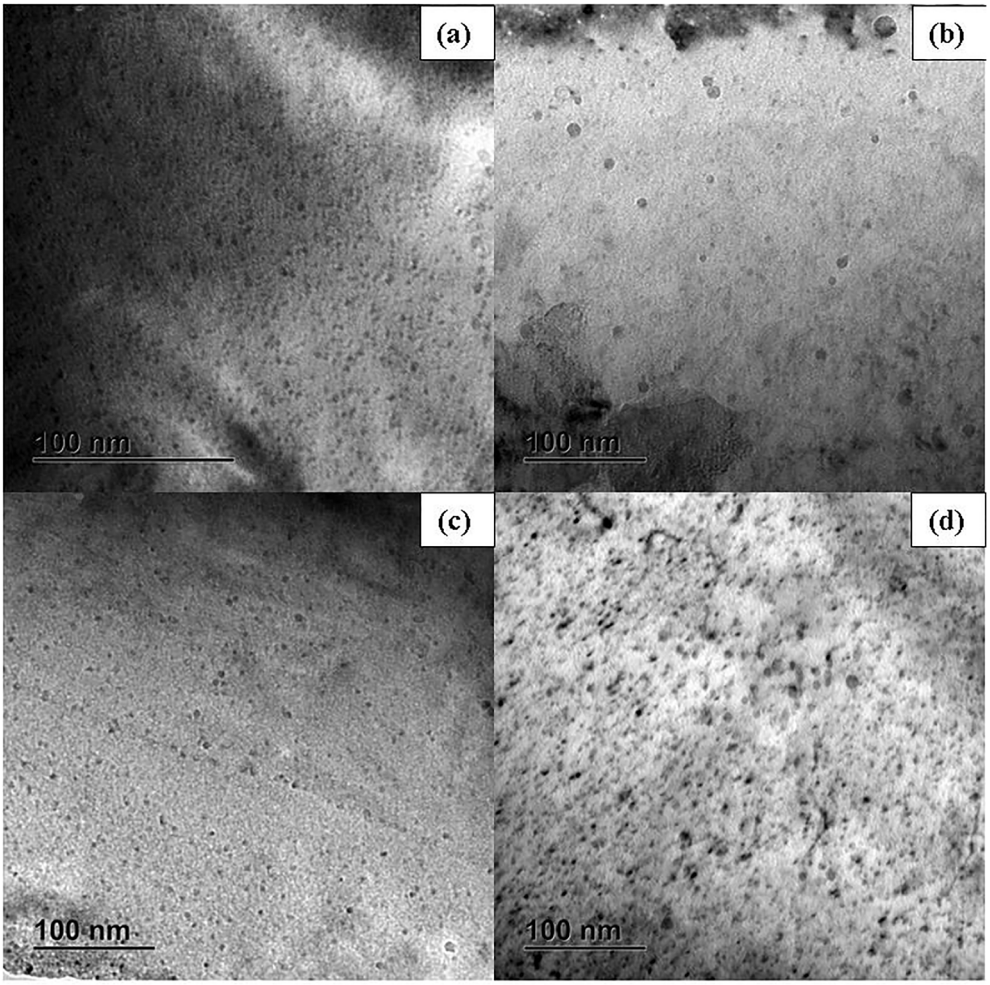

Fig. 12. Representative TEM images showing oxide inclusions in ODS Eurofer irradiated with Xe ions to (a) 1×10^{13} cm^{-2}, (b) 1×10^{14} cm^{-2} and with Au ions to (c) 1×10^{11} cm^{-2} and (d) 5×10^{12} cm^{-2}.

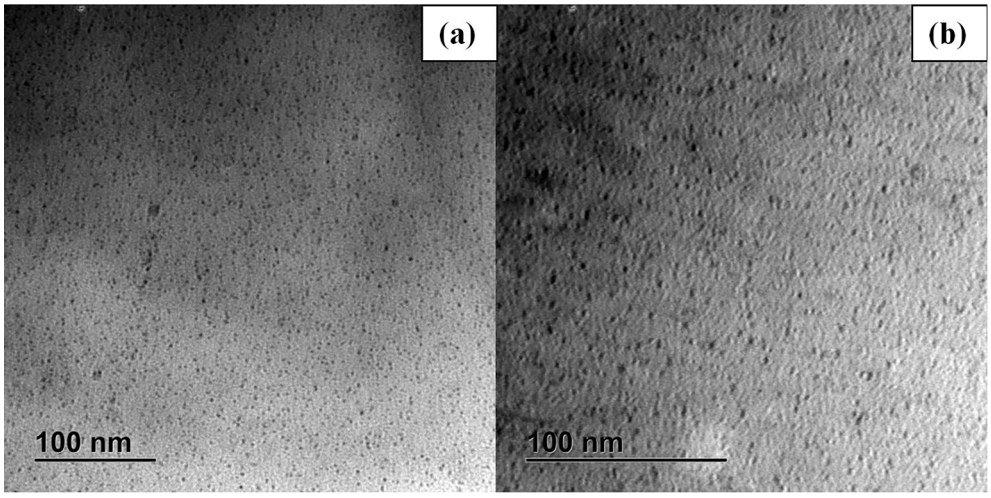

Fig. 13. TEM images of oxide inclusions in ODS 13.5Cr – 0.3Ti steel irradiated with (a) Xe ions to 1×10^{14} cm^{-2} and (b) Au ions to 5×10^{12} cm^{-2}.

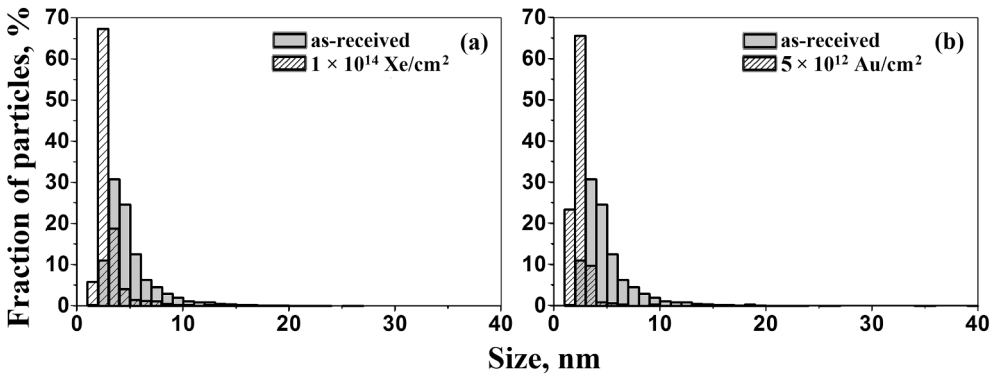

Fig. 14. Size distribution of oxide inclusions in ODS 13.5Cr – 0.3Ti steel before (gray) and after irradiation (shaded) with (a) Xe ions up to 1×10^{14} cm^{-2} and (b) Au ions to 5×10^{12} cm^{-2}.

Table 4
Average size and number density of oxide inclusions in ODS 13.5Cr – 0.3Ti steel irradiated with Au and Xe ions. The quantitative analysis is based on TEM images obtained with a FEI Tecnai F20 microscope.

Type of ions	Au	Xe
Fluence, cm^{-2}	5×10^{12}	1×10^{14}
Oxide size, nm	2 ± 1	3 ± 1
Oxide number density, 10^{22} m^{-3}	6.0 ± 0.6	7.6 ± 0.8

~8 nm while in smaller inclusions no indication for amorphization was found. The average track size increases with electronic energy loss. The number density of the tracks is, within the experimental uncertainties, in agreement with the ion fluence up to track overlapping (i.e., up to 1×10^{13} cm^{-2} for Xe ions). In both, ODS Eurofer and ODS 13.5Cr-0.3Ti steel samples, the irradiation led to partial dissolution of large oxide inclusions resulting in an increase of the number of small inclusions (<5 nm). It can be concluded, that the smaller average size of the oxide inclusions in the initial state of ODS 13.5Cr – 0.3Ti steel compared to the oxides in ODS Eurofer steel yields a greater stability of the steel under

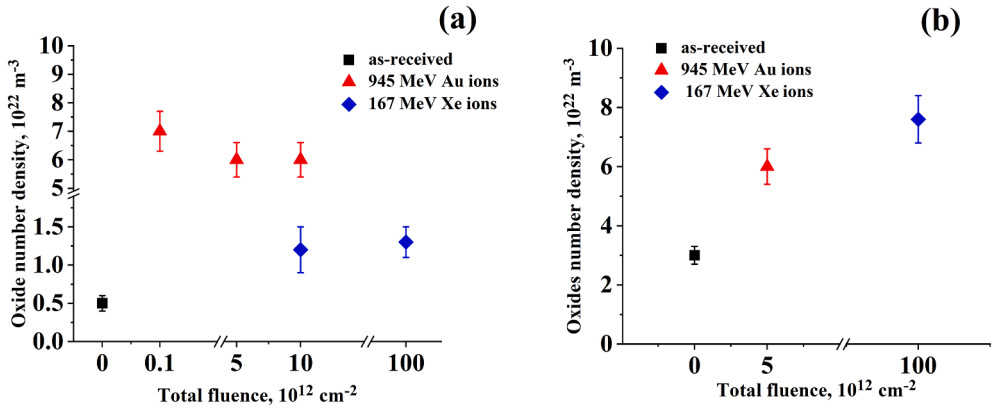

Fig. 15. Number density of oxides for a) ODS Eurofer and b) ODS 13.5Cr – 0.3Ti in as-received state and after irradiation with 945 MeV Au and 167 MeV Xe ions to different fluences. (Colored image for online version).

grows. According to a previous atom probe tomography study [25], investigated ODS steels contain a high number density (about 10^{23} m^{-3}) of 2–6 nm nanoclusters enriched in Y, O, V and N in case of Eurofer ODS and enriched in O, Ti, Y and V in case of ODS 13.5Cr – 0.3Ti. Atomic probe tomography revealed that in a supersaturated matrix the irradiation with low-energy ions can lead to the evolution of large clusters into nano-oxide particles. It is thus reasonable to assume that nucleation of small oxides also occurs due to inelastic interaction with Au and Xe ions. It seems that the nucleation of oxides does not depend on the mechanism of how large oxides dissolve under irradiation, although the energy loss process of swift and low-energy heavy ions is very different.

7. Conclusions

Using high-resolution transmission electron microscopy, we studied the microstructure of ODS Eurofer and ODS 13.5Cr-0.3Ti steels irradiated with 167 MeV Xe ions (1×10^{13} and 1×10^{14} cm^{-2}) and with 945 MeV Au ions Au ions (1×10^{11}, 5×10^{12}, and 1×10^{13} cm^{-2}). In ODS Eurofer, amorphous tracks are formed in oxide inclusions larger than swift ion irradiation.

CRediT authorship contribution statement

Sergey V. Rogozhkin: Conceptualization, Writing - original draft, Writing - review & editing, Formal analysis. **Aleksei A. Bogachev:** Writing - original draft, Writing - review & editing, Investigation, Formal analysis. **Alexander A. Nikitin:** Investigation, Writing - review & editing. **Alexander L. Vasiliev:** Investigation. **Michael Yu. Presnyakov:** Investigation. **Marilena Tomut:** Writing - review & editing. **Christina Trautmann:** Conceptualization, Writing - review & editing.

Declaration of Competing Interest

The authors declare that they have no known competing financial interests or personal relationships that could have appeared to influence the work reported in this paper.

Acknowledgements

This study was supported by FAIR-Russia Research Center and was undertaken in the NRC 'Kurchatov Institute' – ITEP. We also acknowledge the KAMIKS facility (http://kamiks.itep.ru) of the NRC 'Kurchatov Institute' – ITEP for providing access to the instruments at their laboratories. Sample preparation using focused ion beam methods was performed on the equipment of the resource center NANOZOND NRC "Kurchatov Institute" (http://www.rc.nrcki.ru/pages/main/nanozond/). Irradiations with Au ions were carried out at the M3-beam line of the UNILAC at the GSI Helmholtzzentrum für Schwerionenforschung, Darmstadt (Germany) in the frame of FAIR Phase-0. The authors would like to thank Dr. V.A. Skuratov for sample irradiation with 167MeV Xe at the accelerators IC-100 (JINR, Dubna) and for valuable discussion of the presented results. The materials were provided by KIT Karlsruhe, Germany.

References

[1] A.A. Dunlop, G. Jaskierowicz, P.M. Ossi, et al., Transformation of graphite into nanodiamond following extreme electronic excitations, Phys. Rev.B, Condensed Matter. 76 (15) (2007) 1–14.
[2] F.F. Komarov, Damage and track formation in solids irradiated by super-high energy ions, Phys. Usp. 46 (2003) 1253–1282.
[3] M. Lang, R. Devanathan, M. Toulemonde, C. Trautmann, Advances in understanding of swift heavy-ion tracks in complex ceramics, Curr. Opin. Solid State Mater. Sci. 19 (1) (2015) 39–48.
[4] A. Barbu, P. Pareige, V. Jacquet, Precipitation of copper in iron under swift ion irradiations, Nucl. Instr. Meth. Phys. Res. Sect. B Beam Interact. Mater. At. 146 (1998) 278–284.
[5] G.S. Khara, S.T. Murphy, D.M. Duffyet, Dislocation loop formation by swift heavy ion irradiation of metals, J. Phys.: Condens. Matter 29 (2017), 285303.
[6] H. Dammak, A. Dunlop, TEM observations of iron and nickel foils irradiated by MeV fullerenes at room temperature, Nucl. Instr. Meth. Phys. Res. Sect. B Beam Interact. Mater. At. 146 (1–4) (1998) 285–289.
[7] M. Toulemonde, C.h. Dufour, A. Meftah, et al., Transient thermal processes in heavy ion irradiation of crystalline inorganic insulators, Nucl. Instr. Meth. Phys. Res. Sect. B Beam Interact. Mater. At. 166–167 (2000) 903–912.
[8] G. Szenes, Thermal spike analysis of interface mixing induced by swift heavy ions, Appl. Phys. Lett. 81 (24) (2002) 4622–4624.
[9] R.A. Rymzhanov, N.A. Medvedev, A.E. Volkov, Effects of model approximations for electron, hole, and photon transport in swift heavy ion tracks, Nucl. Instr. Meth. Phys. Res. Sect. B Beam Interact. Mater. At. 388 (2016) 41–52.
[10] V.A. Skuratov, V.V. Uglov, J. O'Connell, A.S. Sohatsky, J.H. Neethling, S. V. Rogozhkin, Radiation stability of the ODS alloys against swift heavy ion impact, J. Nucl. Mater. 442 (2013) 449–457.
[11] V.A. Skuratov, A.S. Sohatsky, J.H. O'Connell, K. Kornieieva, A.A. Nikitina, V. V. Uglov, J.H. Neethling, V.S. Ageev, Latent tracks of swift heavy ions in $Cr_{23}C_6$ and Y-Ti–O nanoparticles in ODS alloys, Nucl. Instr. Meth. Phys. Res. Sect. B Beam Interact. Mater. At. 374 (2015) 102–106.
[12] V.A. Skuratov, A.S. Sohatsky, J.H. O'Connell, K. Kornieieva, A.A. Nikitina, J. H. Neethling, V.S. Ageev, M. Zdorovets, A.D. Volkov, Stability of Y-Ti-O nanoparticles in ODS alloys during heat treatment and high temperature swift heavy ion irradiation, Phys. Status Solidi C 13 (10–12) (2016) 927–931.
[13] M.-L. Lescoat, I. Monnet, J. Ribis, P. Dubuisson, Y. de Carlan, J.-M. Costantini, J. Malaplate, Amorphization of oxides in ODS materials under low and high energy ion irradiations, J. Nucl. Mater. 417 (2011) 266–269.
[14] I. Monnet, C. Grygiel, M.L. Lescoat, et al., Amorphization of oxides in ODS steels/ materials by electronic stopping power, J. Nucl. Mater. 424 (1–3) (2012) 12–16.
[15] B.D. Begg, N.J. Hess, W.J. Weber, R. Devanathan, J.P. Icenhower, S. Thevuthasan, B.P. Mc Grail, Heavy-ion irradiation effects on structures and acid dissolution of pyrochlores, J. Nucl. Mater. 288 (2001) 208–216.
[16] S.X. Wang, L.M. Wang, R.C. Ewing, K.V. Govindan Kutty, Ion irradiation of rare-earth- and yttrium-titanate-pyrochlores, Nucl. Instr. Meth. Phys. Res. Sect. B Beam Interact. Mater. At. 169 (2000) 135–140.
[17] J. Ribis, M.L. Lescoat, Y. De Carlan, et al., Stability of nano-oxides upon heavy ion irradiation of an ODS material, J. Nucl. Mater. 417 (1–3) (2011) 262–265.
[18] R. Lindau, A. Möslang, M. Rieth, et al., Present development status of EUROFER and ODS-EUROFER for application in blanket concepts, Fusion Eng. Des. 75–79 (2005) 989–996.
[19] R. Lindau, A. Möslang, M. Schirra, et al., Mechanical and microstructural properties of a hipped RAFM ODS-steel, J. Nucl. Mater. 307–311 (2002) 769–772.
[20] P. He, M. Klimenkov, R. Lindau, A. Möslang, Characterization of precipitates in nanostructured 14% Cr ODS alloys for fusion application, J. Nucl. Mater. 428 (2012) 131–138.
[21] M. Klimiankou, R. Lindau, A. Moslang, HRTEM Study of yttrium oxide particles in ODS steels for fusion reactor application, J. Cryst. Growth 249 (2003) 381–387.
[22] M. Klimenkov, R. Lindau, A. Möslang, New insights into the structure of ODS particles in the ODS-Eurofer alloy, J. Nucl. Mater. 386–388 (2009) 553–556.
[23] J.F. Ziegler, J.P. Biersack, M.D. Ziegler, SRIM,, The Stopping and Range of Ions in Matter, Lulu Press Co, USA, NC, 2015, p. 398 p..
[24] V.A. Skuratov, A.S. Sohatsky, J.H. O'Connell, K. Kornieieva, A.A. Nikitina, J. H. Neethling, V.S. Ageev, Swift heavy ion tracks in $Y_2Ti_2O_7$ nanoparticles in EP450 ODS steel, J. Nucl. Mater. 456 (2015) 111–114.
[25] S. Rogozhkin, A. Bogachev, O. Korchuganova, et al., Nanostructure evolution in ODS steels under ion irradiation, Nuclear materials and energy 9 (2016) 66–74.